Erosion and redeposition patterns on entire erosion marker tiles after exposure in the first operation phase of WEST

M Balden, M Mayer, B Bliewert, E Bernard, M Diez, M Firdaouss, M Missirlian, B Pégourié, M Richou, H Roche, et al.

Erosion and redeposition patterns on entire erosion marker tiles after exposure in the first operation phase of WEST

Physica Scripta

OPEN ACCESS

RECEIVED
4 June 2021

REVISED
1 August 2021

ACCEPTED FOR PUBLICATION
26 August 2021

PUBLISHED
7 September 2021

PAPER

Erosion and redeposition patterns on entire erosion marker tiles after exposure in the first operation phase of WEST

M Balden[1,*], M Mayer[1], B Bliewert[1], E Bernard[2], M Diez[2], M Firdaouss[2], M Missirlian[2], B Pégourié[2], M Richou[2], H Roche[2], E Tsitrone[2], C Martin[3], A Hakola[4] the WEST Team[5]

[1] Max-Planck-Institut für Plasmaphysik, Boltzmannstr. 2, 85748 Garching, Germany
[2] CEA, IRFM, F-13108, Saint-Paul-Lez-Durance, France
[3] Aix-Marseille Université, CNRS, PIIM UMR 7345, F-13397 Marseille, France
[4] VTT Technical Research Centre of Finland Ltd, P O Box 1000, FI-02044, VTT, Finland
[5] See http://west.cea.fr/WESTteam
[*] Author to whom any correspondence should be addressed.

E-mail: Martin.Balden@ipp.mpg.de

Keywords: plasma-wall interaction, WEST, erosion and deposition, RBS and NRA, SEM and EDX, tungsten fuzz, arcing

Abstract

The net erosion and deposition patterns in the inner and outer divertor of WEST were determined after different experimental campaigns (C3 and C4) of the first operational phase using ion beam analyses and scanning electron microscopy techniques. The analyses were performed on four entire tiles from inertially cooled, W-coated divertor units with an additional Mo marker coating covered with a further W coating. Strong erosion occurred at the expected location of the inner and outer strike line area with a campaign-averaged net erosion rate of >0.1 nm s^{-1}. On the high field side of the inner strike line area, thick deposited layers were found (>10 μm; growth rate >1 nm s^{-1}), mainly composed of B, C, O, and W. Additionally, strong arcing was observed in this region. At the end of the C4 campaign, He discharges were performed to study the He-W interaction. Although the conditions for nanotendrils, i.e. fuzz formation were fulfilled around the outer strike line position, neither nanotendrils nor He bubbles (>10 nm) were observed at this area.

1. Introduction

Erosion and redeposition are important aspects when analyzing plasma-wall-interactions in fusion plasma devices. The major erosion process is physical sputtering by the plasma main species (e.g. hydrogen or helium) and its impurities (e.g. oxygen, carbon, and boron). The eroded material is transported by the plasma around the device and can subsequently be redeposited in the vessel. Due to the interplay of erosion and deposition, which can strongly vary during experimental campaigns encompassing a wide range of plasma conditions, a complex situation of erosion-deposition occurs. The processes and their interplay have been thoroughly studied in the past for various experimental devices [1–6], and will remain on the agenda for follow-up studies on existing and new devices to validate simulation tools and to confirm their predictive capability for future machines, like ITER or DEMO [7–11].

The WEST project is devoted to test the tungsten (W) divertor technology selected for ITER [12] in an integrated tokamak environment [13, 14]. For that, the carbon-based limiter tokamak 'Tore-Supra', operating with L-mode discharges from 1988 to 2012, was transformed into an X-point divertor configuration. After a long-lasting construction phase implementing new poloidal coils to achieve diverted operation and an all-tungsten cladding, the first plasma was achieved at the end of 2016 [15]. Thereafter, the 1st operational phase with five experimental campaigns (C1-C5) was completed in early 2021.

WEST started its operation with a mix of actively cooled and inertially cooled plasma-facing units (PFUs) in the lower divertor. The number of actively cooled ITER-like tungsten (W) monoblock chains was successively increased in phase 1, and in phase 2 only actively cooled PFUs will be installed in the lower divertor. The inertially cooled PFUs were W-coated graphite tiles. Some of these were specially coated with an additional

molybdenum (Mo) layer covered by a further W layer to be used as marker tiles, i.e., to allow determining the thickness change of the top W layer and, therefore, the net erosion resulting from the competition between the erosion and deposition processes. The analyses of these tiles deliver complementary data to the spectroscopic studies of W performed during plasma operation, allowing to assess the so-called gross erosion, as this signal integrates all eroded W atoms, including the promptly redeposited ones. The W spectroscopic emission profile [16] shows an in/out asymmetry in the divertor. Additionally, significant changes in infrared (IR) emissivity of these PFUs were observed [17].

In all five experimental campaigns of the 1st operational phase, the discharges were executed in deuterium (D), except at the end of C4. This part of the campaign was devoted to a dedicated helium (He) campaign to investigate He-W interactions, particularly with respect to the variation of W erosion and scrape-off-layer (SOL) widths between He and D plasmas and to the W fuzz formation [18]. The changeover between He and D in a full-W device [19] was studied. The conditions promoting W fuzz formation were reached around the outer strike line [18].

This paper presents 1st results of post-mortem analysis using ion beam analysis and different microscopy techniques of the W erosion and redeposition patterns in the full-tungsten plasma-facing environment of WEST for some marker tiles removed after the C3 and C4 campaign.

2. Experimental

2.1. Prelude to WEST and samples

The lower divertor of WEST consists of 12 sectors each containing 38 components toroidally distributed. In the campaigns C1 to C4, only one sector was partially equipped with ITER-like PFUs [12] each consisting of 35 W monoblocks of ≈12 mm width in poloidal direction brazed on a copper (Cu) tube. All the other sectors were composed of inertially cooled graphite tiles with width in toroidal direction ranging from 26 mm (in the HFS) to 33 mm (in the LFS). They consists of two tiles with a gap between them located in the private flux region (PFR). These graphite tiles of ≈330 mm and ≈260 mm length in poloidal direction for the inner and outer tiles, respectively, were coated with ≈12 μm W on top of a ≈3 μm Mo interlayer by PVD CMSII [20].

Eight of these 'standard' tiles were coated additionally with a thin Mo interlayer and a W cover layer (arc-discharge sputtering [21]). This thin buried Mo layer serves as a marker for investigating campaign-integrated W net erosion behavior by determining the remaining W cover layer thickness. The initial W marker thickness varies along the length of the tiles between ≈1 μm and ≈2 μm. These eight so-called marker tiles were mounted before the C1 campaign. They were placed at the toroidal position where the surface loading is most extreme due to the magnetic ripple modulations [18]. The toroidal positions for maxima of these modulations at the inner strike line position (ISP) and the outer strike line position (OSP) are different, i.e., the maximum of the ISP is at the toroidal position of the minimum of the OSP and vice versa. Figure 1 shows a photo of the sector equipped with the marker tiles after the C3 campaign as well as cartoons of the layer structure of the standard and marker tiles and the design of the tiles. Also shown are the starting points and the direction of the S-coordinate of the inner and outer divertor tiles. The S-coordinate is used throughout this study as a reference and is given with its direction in the following figures.

Two marker tiles were removed after the C3 campaign, four marker tiles after the C4 campaign, and the remaining two stayed until the end of the C5 campaign. The tiles located at the maximal flux area removed after C3 and C4 (sample naming C3-22o and C3-34i for tiles removed after C3, C4-20o and C4-32i for tiles removed after C4) were analyzed in this study as well as one standard tile (C4-19o-s) mounted directly beside C4-20o, which was removed also after C4. The other four marker tiles are not yet analyzed (two removed after C4 and the two final ones after C5). The accumulated D plasma duration (including limiter ramp-up and ramp-down phases as well as flat top divertor phases) was ≈8900 s for C1-C3. In addition to D plasma discharges in C4 with ≈10000 s accumulated plasma duration, He plasma discharges were performed in two phases at the end of C4 with an accumulated plasma duration of ≈3000 s, out of which 2000 s were dedicated to study the W-He interactions just before the end of C4. Boronisations were started in C3 (3 times) to extend the operational domain, and were regularly performed in C4 (13 times) and C5 (3 times), with none during the He phases performed at the end of C4.

A long pulse scenario (up to ≈1 min) was developed to study plasma-wall interactions. The flat top divertor heat flux (at the most loaded OSP area) was steadily increased up to ≈6 MW m^{-2} [22]. Although WEST was mainly operated in L mode (without edge localized modes, ELMs), a significant number of discharges (≈2000) was terminated by disruptions. The long pulse operation was partially performed with nitrogen (N) seeding. Small amounts of N were also used to initiate standard plasmas in D.

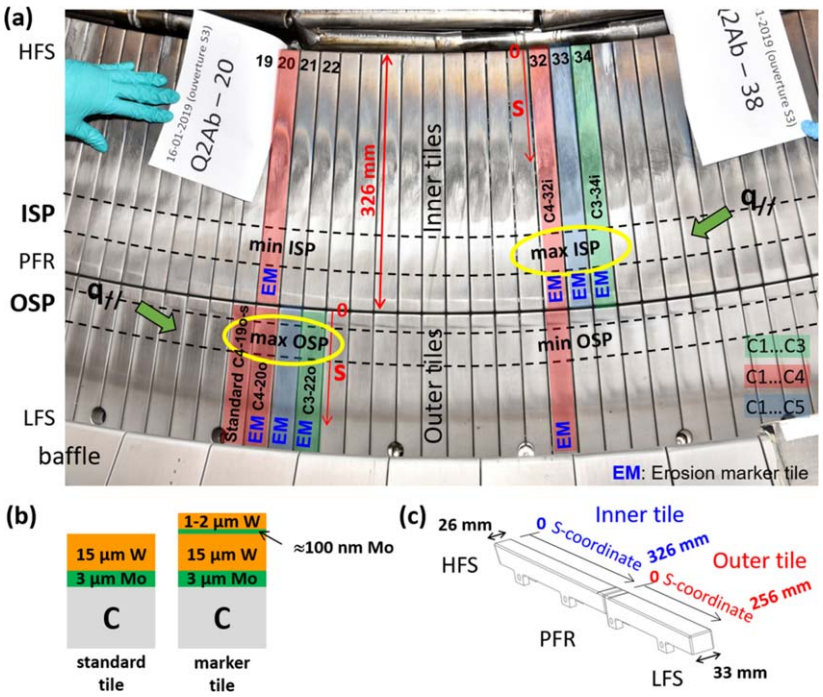

Figure 1. (a) Photo of the lower divertor sector equipped with the marker tiles after the C3 campaign. Overlays mark (i) the PFU numbers (top), (ii) the marker tiles (EM for erosion marker tiles) and the identifier numbers of the analyzed marker tiles as well as of the additional analyzed standard tile, (iii) the campaigns, in which the tiles of interest were mounted inside WEST (color-coded), (iv) the expected positions of the inner (ISP) and outer strike line area (OSP) obtained from the magnetic reconstruction of the applied discharge scenarios with the most loaded areas circled in yellow and the incident flux direction leading to shadowed regions on the opposite side for inner and outer tiles, (v) S-coordinate origins and direction pointing from high field side (HFS) to low field side (LFS). (b) Cartoons of the layer structure of the standard and marker tiles. (c) Drawing of W-coated inertial graphite tiles with some labelling (see (a)).

2.2. Ion beam analyses

The ion beam analyses were carried out in the 'Bombardino' analysis chamber, which allows to handle samples up to a maximum length of about 400 mm at the tandem accelerator at IPP, Garching [23]. The analysis positions were placed along the central line of the tiles, mostly with a distance of 12.5 mm in poloidal direction. The ion beam spot size was ≈2 mm^2. For each analyzed position, Rutherford backscattering spectrometry (RBS) using 3.0 MeV protons at 165° and 2.5 MeV ^{3}He ions at 165° as well as nuclear reaction analyses (NRA) using 2.5 MeV ^{3}He ions at 150° were performed. The RBS and NRA data were fitted in a self-consistent way by using the SIMNRA software [24] to obtain the total amount of W above the thin Mo layer (remnant of top W coating and redeposited W) and the amounts of boron (B), carbon (C), D, and oxygen (O) in the deposited layers. The fitted stack of layers with different composition on top of the pure W and Mo layers takes into account the roughness and thickness variations. The ratio B/C is assumed to be constant in the entire deposited layer even beyond the information depth of NRA of ≈1.5×10^{23} atoms m^{-2} in light elements (about 1.5 μm). The D amount can be observed depth-resolved up to a depth of about 2.2×10^{23} atoms m^{-2} (about 3 μm) in W. The Mo and W marker layers are best visible in the RBS measurements. Their quantification is restricted by the surface roughness and the presence of deposition layers, which smears out their signals. At some measuring positions, the thickness of the deposited layer is too thick, so that the thin Mo layer cannot be detected anymore. Note, as O does not exhibit a nuclear reaction at the used ion beam energies and its RBS signal is weak and overlapping with other elements, its amount was used as a free parameter, i.e., any signal from medium Z metals, e.g. Cu, contributes to it. Nevertheless, the total thickness of the deposited layer by RBS and NRA is a robust number (within ≈20%). Figure 2 summaries the amounts of W, B, C, O, and D obtained by RBS and NRA for the marker tiles analyzed in the frame of this study.

2.3. Scanning electron microscopy and confocal laser scanning microscopy

Scanning electron microscopy (SEM) assisted by energy dispersive x-ray spectroscopy (EDX) to determine the elemental composition at the electron beam position were performed on the surface as well as on focused ion beam (FIB) prepared cross-sections of the samples. The AURIGA facility at IPP, Garching, is capable of investigating the entire WEST tiles without cutting them into smaller pieces [25]. Several FIB-prepared cross-sections were analyzed on the four marker tiles as well as on one exposed standard tile and an unexposed spare

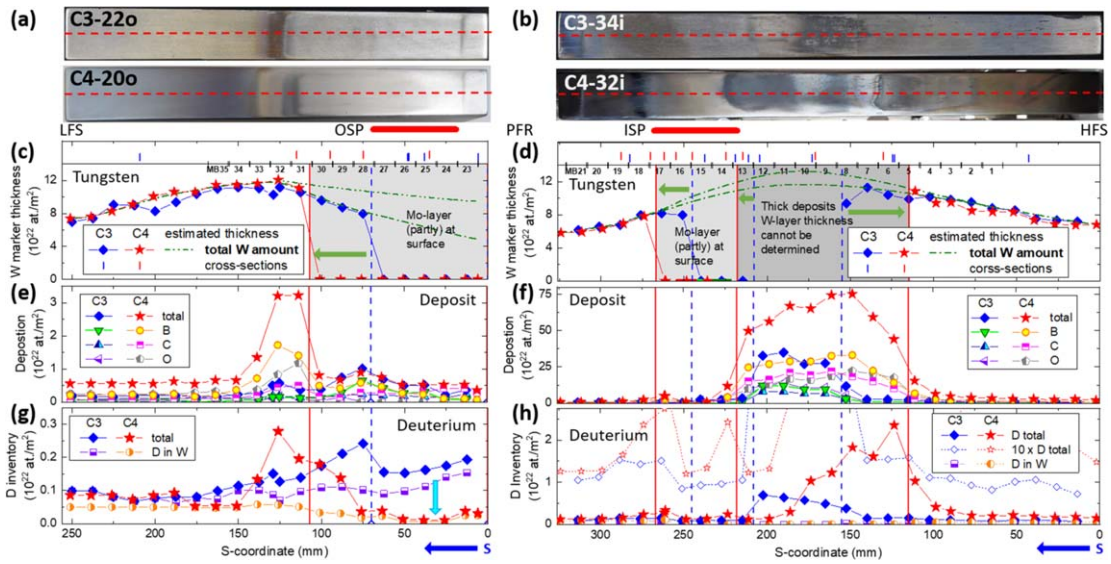

Figure 2. (a), (b) Photos of the four analyzed marker tiles; the positions of the ISP and OSP obtained from magnetic reconstruction of the applied plasma scenarios averaged of the C3 and C4 campaign are marked below the photos. (c), (d) total W amount above the Mo marker layer along the central line (poloidal direction) of the marker tiles. The green dashed dotted lines represent two estimated initial thicknesses of the W top layer. Assuming the density of bulk W, 6.3×10^{22} atoms m^{-2} corresponds to ≈ 1 μm. The S-coordinates of the analyzed FIB-prepared cross-sections are marked in the box above the graphs (vertical bars) as well as the respective positions and numbering of W monoblocks of the ITER-like PFUs. The light grey and dark grey highlighted areas indicate the range of strong erosion and thick deposition after C4, respectively, framed by red vertical lines, while the analogous areas after C3 are marked by dashed blue vertical lines. The green horizontal arrows indicate the shift of the edge of the strongly eroded areas and the area with thick deposition between C3 and C4. (e-h) Amount of B, C, D, and O as well as the sum of these four signals along the central line of the marker tiles. The D amount into the W coating is assigned as 'D in W'.

standard tile. SEM images for electron beam energies of 5 keV and 20 keV were recorded with secondary electron (SE) and backscattered electron (BSE) detectors. In addition to magnification series of the areas before cross-sectioning and of several further positions, large area stitching scans with the ATLAS system (Fibics Inc.) were recorded to enable microscopic post-analyses when needed to assist future analyses on smaller samples after cutting the marker tiles.

The roughness, mainly a remnant from the grinding grooves and the porosity of the graphite tiles before coating, affects the erosion/deposition pattern and, therefore, the SEM analyses especially of the FIB-prepared cross-sections. Therefore, for most of the SEM analyzed positions, confocal laser scanning microscopy (CLSM) [25] data were additionally measured to quantify the height profile. The surface roughness, S_a, for unexposed standard tiles was ≈ 2 μm.

3. Results and discussion

3.1. RBS and NRA results assisted by SEM analyses

In figure 2, the RBS and NRA results of the four analyzed marker tiles are compiled together with photos of them and the S-coordinate of the FIB-prepared cross-sections. The amounts of W after C4 outside the highlighted areas in figures 2(c), (d) agree well with those after C3, which represent the initial thickness of the top W layer. The initial thickness is mainly between 1 μm and 2 μm. For these areas, no significant interaction with the plasma is expected, as they are located several centimeters away from the applied strike line positions. In particular, the area located on the LFS of the outer tile is magnetically shadowed from the plasma by the baffle ($S \approx 250$ mm). An equivalent thickness (with some variation of up to 4 μm) is observed with SEM on FIB-prepared cross-sections (figure 3(e)), where the Mo marker layer appears as edgy dark lines following the crystalline surface of the ≈ 12 μm W coating (figure 3).

For the light grey areas in figures 2(c), (d), where the W amount is zero, the RBS spectra as well as the SEM/EDX analyses indicate clearly that these areas are so strongly eroded that the thin Mo layer intersects the surface (figures 3(a)–(c)). From the plasma duration (including both limiter and divertor phase), a lower limit for the campaign-averaged net erosion rate of >0.1 nm s^{-1} can be assessed for C3, as well as for C4 by considering the erosion of the enlarged erosion area ($S = 70$–110 mm; see green, horizontal arrows in figure 2). This lower limit of the net erosion rate is in the same range as observed for ASDEX Upgrade [26] and Wendelstein 7-X [27]. An upper value for the net erosion rate can be estimated to be <0.5 nm s^{-1}, taking into account the partial remnant

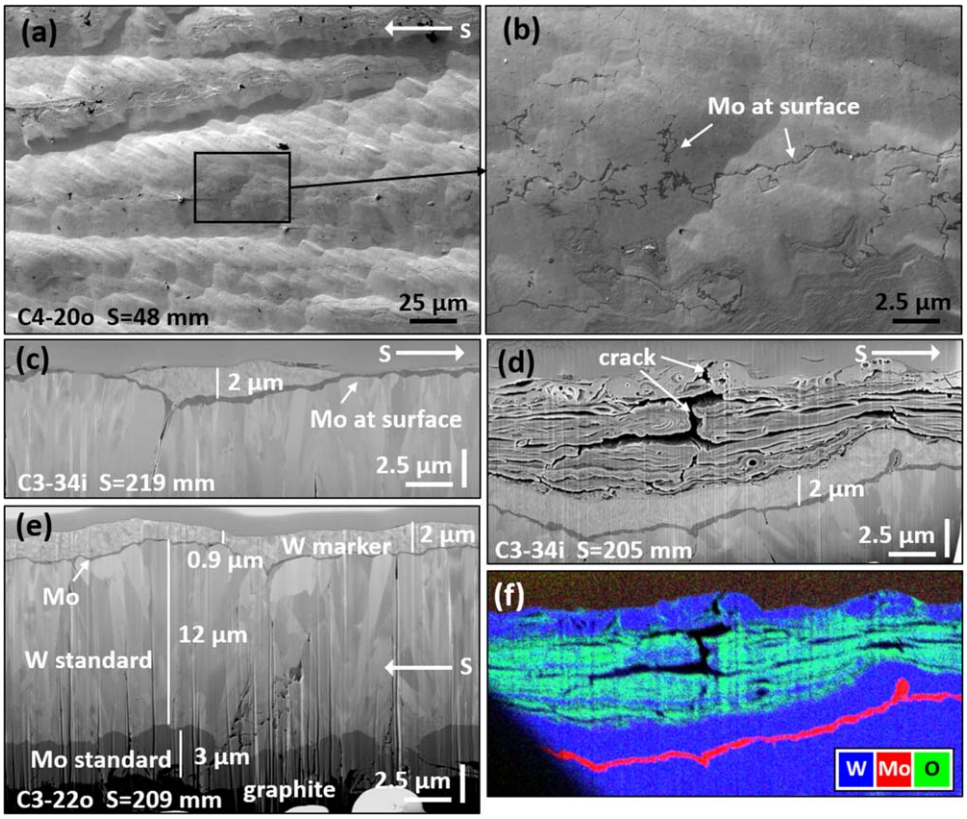

Figure 3. Analysis of marker tiles removed after the C3 campaign (tile number and S-coordinate are indicated in the images). Surface images (untilted) of an area of strong erosion in two magnifications (a,b) with Mo marker coating visible on the surface as edgy, dark lines and images of FIB-prepared cross-sections of area with strong erosion (c), area with thick, layered redeposition (d) and of the quasi initial marker layer (e). (f) shows an EDX mapping of the region of (d) indicating a large fraction of W in the deposit, which is especially high in the top layer at the surface. Note, the cross-section planes are tilted by 36° to the viewing plane, and all SEM images are taken with the SE detector.

of the top W layer, the uncertainties in the initial marker coating thickness, impact of surface roughness etc. The shift of the strongly eroded area is supported by the expected OSP and ISP from the magnetic reconstruction of the performed plasma scenarios during the campaigns.

The initial W thickness above the Mo marker layer is extrapolated for the regions of strong erosion and thick deposition, resulting in an upper and lower reasonable value (figures 2(c), (d)). As it is not clear whether the S-coordinate range between 70 and 110 mm on the outer C3 tile is already affected by erosion or not, the spread of the estimate is higher than for the inner tile.

The transition from strong erosion to the thick, layered redeposition (figures 2(d), (f)) on the inner tiles is remarkable sharp, within a few millimeters. The thickness of the redeposition reaches more than 10 μm after C3 on the inner tile (figures 3(d) and 4(b)) and is even thicker after C4 (roughly doubled, figures 2(e), (f)). This thickness reaches up to the maximal analyzing depth for the used beam energy. Overall, a campaign-averaged deposition rate of >1 nm s^{-1} is observed. Some layers of the deposits are dominated by W (figures 3(f) and 5(b), (c), (e))), while others show a large amount of O (e.g. dark lines in figures 3(d) and 5(b), (c)). Oxygen may be incorporated into the deposit layers during plasma operation, but may originate also from oxidation of the layers during exposure to air, resulting in a larger geometrical thickness. Oxygen can penetrate probably easily into the layers due to their high porosity. A quantification of the origin of oxygen is not possible. Unfortunately, B is hardly detectable with EDX due to the strong absorption of its low energy x-ray line. But it is believed that B is often present where a large amount of O is observed. Nevertheless, B is clearly found at some places. The higher B amount found after C4 reflects the higher number of boronisations. This result is also observed on the deposits collected on the ITER-like PFUs [28].

In addition to the expected elements (B, C, D, W, Mo, O), N, Cu and, after C4, silver (Ag) are frequently detected in low amounts in the deposits. Cu can be originated from the lower hybrid heating system or from the Cu substrate at the baffle or the upper divertor after delamination of the W coating, while Ag coatings are used on the ICRH antenna. Nitrogen was used as seeding gas and for start-up in some plasma scenarios. The surface of the W-dominated top layer of the deposit is hardly distinguishable from a modified surface of the W coating

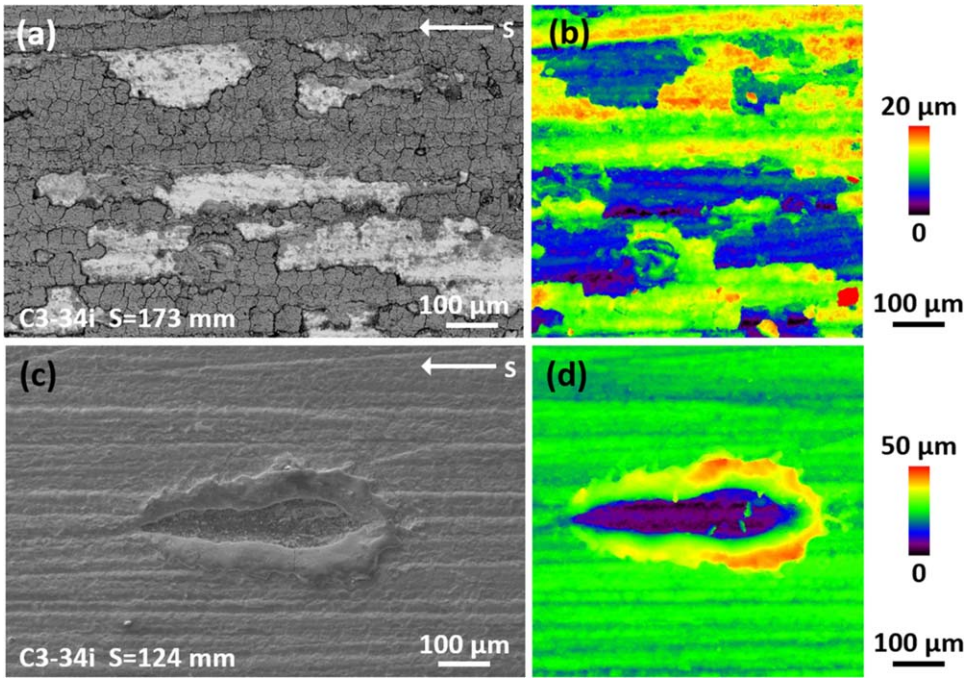

Figure 4. Analysis of marker tiles removed after the C3 campaign (tile number and S-coordinate are indicated in the images). Surface images of (a) an area with thick, layered redeposits partially peeled off (BSE, untilted), and (c) an area with a strong arc which burned through the whole stack of coatings (SE, untilted). (b), (d) CLSM height data of the same areas as shown in (a) and (c), respectively.

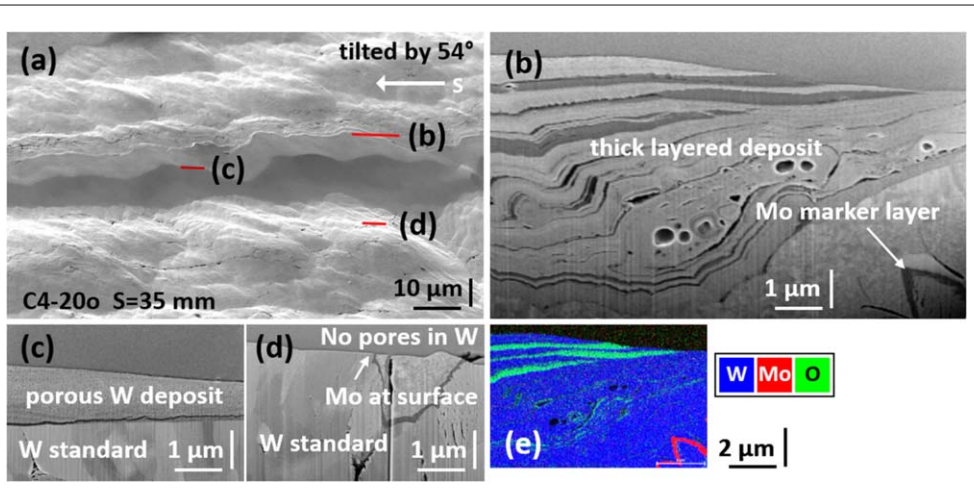

Figure 5. Analysis of marker tiles removed after the C4 campaign (tile number and S-coordinate is indicated in the image). (a) Tilted surface image from the OSP, for which the conditions of fuzz formation during the He phase of C4 are fulfilled. (b)–(d) SEM images of FIB-prepared cross-sections of positions marked in (a). (e) is an EDX mapping of the region of (b) showing the multilayer structure with several of them with a large fraction of W and other with O. Note, the cross-section planes are tilted by 36° to the viewing plane, and all SEM images are taken with the SE detector.

and hide layers of other composition. Larger areas of this thick deposit show a crack network, which does not penetrate into the W-coating below. Partially the deposition layers peeled off (figures 4(a), (b)).

Just beside the outer strike line position (OSP), redeposition is observed, but much thinner than on the inner tile (roughly a factor 20 thinner, figures 2(e), (f)). It has to be stressed that also on the strong erosion areas, significant deposition is observed on the microscopic scale, which follows mostly the grooves of the surface roughness. This is a well-known behavior [29], and an example is given in figure 5. The plasma shaped surface topography shows the directional shaping of the erosion/deposition features (figures 3(a) and 5(a)) due to the interplay of erosion and deposition resulting from the different impact angle distributions of the plasma species and the impurities [30, 31].

The optical impression (figures 2(a), (b)), which also depends strongly on the illumination, is not simply transferable to the erosion/deposition pattern observed with RBS/NRA and SEM. Examples for that are the

brownish feature at S $\approx$ 75 mm on C3-22o or the sharp line at S $\approx$ 80 mm on C4-32i. The W-dominated top layer of the deposit has definitely an effect of the optical appearance and its IR-emissivity (figures 3(f) and 5(b), (c), (e)).

The D depth profile typically consists of a surface peak and a tail reaching into the W substrate with much lower intensity. The D concentration in the W substrate, i.e. beyond the stack of fitted layers with different composition, is usually in the range 0.2 at% to 0.5 at% after C3. This is a typical value for D diffusing into W by D plasma exposure [32]. The ratio of D to the deposited C + B + O varies strongly across the C3 tiles, reaching often the known high value of ≈0.4 [33]. For the C4 tiles, this value is always by at least a factor of two lower. The given total amounts of D (figures 2(g), (h)) are limited to the maximum depth of analysis of about 3 μm in W and up to ≈10 μm in the light element deposits. The D extends much further into the depth in both, i.e., the total D amount is underestimated. The fraction attributed to be stored in the W coating is separately shown in figures 2(g), (h), only the part of the tail which can be attributed to depth definitely reaching the pure W layer. It is noteworthy that the D amount in the W coating in the outer tiles is homogenous and higher than on the inner tiles after C3, but the D is strongly depleted at the OSP after C4 due to the He exposure at higher surface temperatures.

The detailed cross-linking of the observed net erosion and deposition pattern with variations of the plasma conditions and positions is pending and will be done in follow-up publications. This cross-linking is especially of interest for considering the IR-emissivity variation and its evaluation [18].

3.2. Additional observations from SEM analyses

3.2.1. Arcing

Strong arcing is observed on the inner divertor tiles on the HFS of the area with strong erosion (ISP) [34], where deposition dominates and which is the analogous location where arcing is observed in other devices [35, 36]. These arcs burned through the complete stack of coatings into the graphite substrate (figures 4(c), (d)). After C3, the bottom of the traces shows graphite and remnants of the thick Mo coating layer. After C4, these arc traces in the area of thick deposition were all covered by deposits with the typical elongated surface topography following the main impact direction of the plasma (figures 3(a) and 5(a)). This indicates that this type of arcing did not appear anymore at least at the end of C4, e.g., in the He discharges. The density of the arc traces is strongly inhomogeneous, being lower at the upstream side. This inhomogeneity hinders concluding whether such arcing appeared in C4 at all. Beside these large traces visible already by naked eye (figure 2(b), top right corner), many smaller traces still burning into or even through the stack of coatings are present covering about the same area as the large ones. Overall, for large areas on the inner tiles, a surface fraction of above 1% is affected by this strong arcing. Further statistical sound evaluations are required.

In addition to this strong arcing, a 'soft' arcing is overlaid. It covers nearly the complete part of the inner tile on the HFS of the ISP. These soft arcs affect mainly the appearance of the deposited layers and alter the topography only marginally. Mostly ≈10%, but sometimes up to 50% of the surface is affected by them. Furthermore, at the PFR on the inner divertor tile after C4 and on the LFS of the outer strike line area on the outer tile after C4, such soft arcing is observed.

3.2.2. Effect of He discharges at the end of the C4 campaign

At the maximal flux areas of the OSP, the conditions for W fuzz formation are fulfilled during the C4 campaign, although marginally [18, 37]. A He fluence of above 10^{24} He m^{-2} with an energy above 20 eV He^{-1} was accumulated while the samples surface temperature was above 700 °C as obtained from IR data. More details on the evaluation of these conditions can be found in [18]. Special emphasis was therefore put on analyzing the OSP region on the two tiles available after C4 (C4-20o, C4-19o-s). Figure 5 shows the surface of the marker tiles and three cross-sections of areas with and without deposition. The resolution of the obtained SEM images allows to exclude the presence of pores, i.e. He bubbles, with a diameter above 10 nm inside the W of the coating. The typical fuzz tendrils, easily observable with SEM, are clearly absence, too. These results indicate that significant W fuzz formation did not occur in this area during C4 in WEST. Note, the porous W deposit with pores in the tens nanometer range shown in figure 5(c) is also observed after C3, i.e., it cannot be related to the He exposure. Further analyses, e.g. by transmission electron microscopy, are envisaged to extend and confirm these first results.

4. Summary

The net erosion and deposition patterns of the W divertor of the WEST tokamak were determined after the C3 and C4 experimental campaigns. A combination of techniques, RBS, NRA, SEM with EDX and FIB as well as

CLSM, was applied on five entire inertially cooled W-coated graphite tiles after the C3 and C4 campaign. The following conclusions can be drawn:

(i) Both, inner and outer strike line area, are erosion-dominated with a campaign-averaged net erosion rate of >0.1 nm s^{-1}, which is in the same range as observed for ASDEX Upgrade [25] and W7-X [26].

(ii) Thick deposits composed mainly of B, C, O and W of >10 μm for a 5–10 cm wide poloidal band are observed on the high field side of the inner strike area with a sharp transition from the strong net erosion area.

(iii) Outside of this stripe, moderate deposition is observed, even at the strong net erosion areas and in the private flux region.

(iv) The poloidal width of the area of strong erosion and of the thick deposition is enlarged after the C4 campaign compared to the C3 campaign.

(v) Heavy arcing on the high field side destroyed the coating locally. The affected area fraction reaches about 1% at parts of the inner divertor tiles.

(vi) Even if the conditions for W fuzz formation ($>10^{24}$ He m^{-2}, >20 eV He^{-1}, >700 °C) were fulfilled in the He discharges at the end of the C4 campaign on the outer strike line area, no fuzz nor He bubbles are observed, indicating a complex interplay between fuzz formation and erosion/redeposition in the tokamak environment.

The successful quantitative analysis of such complex layer structures as observed at WEST requires the combination of different analytical methods, especially RBS, NRA, SEM with EDX and FIB. The AURIGA and the Bombardino set-up, allowing to analyze entire tiles, are particularly well suited to get a global view of these complex erosion/deposition patterns in a time efficient way after campaign exposure. Further analysis will now be performed on small scale samples to be cut from the tiles, using this first set of results on entire tiles as a guidance. The presented data as well as the more detailed future analyses will be used to benchmark the various simulation activities [7–11], targeted at predicting plasma wall-interaction for ITER and beyond.

Acknowledgments

This work has been carried out within the framework of the EUROfusion Consortium and has received funding from the Euratom research and training programme 2014–2018 and 2019–2020 under grant agreement No 633053. The views and opinions expressed herein do not necessarily reflect those of the European Commission. Part of the work was performed under EUROfusion WP PFC.

Data availability statement

The data that support the findings of this study are available upon reasonable request from the authors.

ORCID iDs

M Balden https://orcid.org/0000-0002-8755-9370
M Mayer https://orcid.org/0000-0002-5337-6963
E Bernard https://orcid.org/0000-0002-9291-7654
M Diez https://orcid.org/0000-0002-8334-3521
M Richou https://orcid.org/0000-0002-8447-868X
C Martin https://orcid.org/0000-0002-4704-3273
A Hakola https://orcid.org/0000-0003-1385-1296

References

[1] Brezinsek S *et al* 2017 *Nucl. Fusion* **57** 116041
[2] Aho-Mantila L *et al* 2012 *Nucl. Fusion* **52** 103007
[3] Hakola A *et al* 2016 *Phys. Scr.* **2016** 014026
[4] Catarino N *et al* 2020 *Phys. Scr.* **2020** 014044
[5] Ding R *et al* 2015 *Nucl. Fusion* **55** 023013
[6] Dai S *et al* 2014 *Nucl. Fusion* **54** 123015

[7] Tokar M Z 2018 *Nucl. Fusion* **58** 016016
[8] Gallo A *et al* 2020 *Phys. Scr.* **2020** 014013
[9] Kirschner A *et al* 2018 *Plasma Phys. Control. Fusion* **60** 014041
[10] Schmid K *et al* 2020 *Nucl. Mater. Energy* **25** 100821
[11] Schmid K *et al* 2015 *Nucl. Fusion* **55** 053015
[12] Hirai T *et al* 2013 *Fusion Eng. Des.* **88** 1798–801
[13] Bucalossi J *et al* 2014 *Fusion Eng. Des.* **89** 907–12
[14] Bourdelle B *et al* 2015 *Nucl. Fusion* **55** 063017
[15] Moreau P *et al* 2020 *IEEE Transaction Plasma Sci.* **48** 1376–81
[16] van Rooij G J *et al* 2020 *Phys. Scr.* **2020** 014060
[17] Gaspar J *et al* 2020 *Nucl. Mater. Energy* **25** 100851
[18] Tsitrone E *et al* 2021 IAEA; with follow-up *Nucl. Fusion* paper (Unpublished; in 1st revision round)
[19] Bisson R *et al* 2021 *Nucl. Mater. Energy* **26** 100885
[20] Firdaouss M *et al* 2017 *Fusion Eng. Des.* **124** 207–10
[21] Lehto S *et al* 2003 *Fusion Eng. Des.* **66–68** 241
[22] Gaspar J *et al* 2021 IAEA; with follow-up *Nucl. Fusion* paper (Unpublished; in 1st revision round)
[23] Mayer M *et al* 2020 *Nucl. Fusion* **60** 025001
[24] Mayer M 2014 *Nucl. Instrum. Methods Phys.* **332** 176–80
[25] Balden M *et al* 2020 *Phys. Scr.* **T171** 014026
[26] Mayer M *et al* 2007 *Phys. Scr.* **T128** 106
[27] Mayer M *et al* 2021 Erosion of tungsten marker layers in W7 *Presented at 18th Inter. Conf. on Plasma-Facing Materials and Components for Fusion applications, Phys. Scr. (in 1st revision round)*
[28] Martin C *et al* 2021 First post-mortem analysis of deposits collected on ITER-like components in WEST after the C_3 and C_4 campaigns *Presented at 18th Inter. Conf. on Plasma-Facing Materials and Components for Fusion applications, Phys. Scr. (in 1st revision round)*
[29] Kallenbach A *et al* 2011 *J. Nucl. Mater.* **415** S19–26
[30] Balden M *et al* 2013 *J. Nucl. Mater.* **438** S220–3
[31] Schmid K *et al* 2010 *Nucl. Fusion* **50** 105004
[32] Ueda Y *et al* 2017 *Nucl. Fusion* **57** 092006
[33] Roth J *et al* 2009 *J. Nucl. Mater.* **390-391** 1–8
[34] Diez M *et al* 2021 In-situ observation of tungsten plasma-facing components after the first phase of operation of the WEST tokamak, Unpublished to *Nucl. Fusion* IAEA (https://doi.org/10.1088/1741-4326/ac1dc6)
[35] Rohde V *et al* 2017 *Nucl. Mater. Energy* **12** 429–32
[36] Rohde V *et al* 2021 *Nucl. Mater. Energy Unpublished (presented at 24th International Conference on Plasma Surface Interactions in Controlled Fusion Devices (PSI 2021)*
[37] De Temmerman G *et al* 2018 *Plasma Phys. Control. Fusion* **60** 044018